

The theory of short-gap breakdown of needle point–plane gaps in air using finite-difference and finite-element methods

G E Georgiou[†], R Morrow[‡] and A C Metaxas[†]

[†] Electricity Utilisation Group (EUG), Department of Engineering, University of Cambridge, Trumpington Street, Cambridge CB2 1PZ, UK

[‡] CSIRO, Division of Telecommunications and Industrial Physics, PO Box 218, Lindfield NSW 2070, Australia

E-mail: geg1000@eng.cam.ac.uk, richard.morrow@tip.csiro.au and acm@eng.cam.ac.uk

Received 13 August 1998, in final form 19 February 1999

Abstract. Numerical results are presented for the formation of breakdown streamers which bridge a 1 mm gap between a positive 50 μm radius hyperboloid point and a plane, when a dc voltage is applied. The results show that, for such gaps, no streamers form at voltages lower than or equal to 2.5 kV and that streamers bridge the gap at higher voltages. The streamer speed and radial dimensions of the streamer are found to linearly increase with the applied voltage and this agrees with what is predicted by existing two-dimensional models. The electric field in the streamer channel behind the streamer head is initially found to be much lower than that for longer gaps and becomes comparable only later in the development of the streamer. The results are obtained using a pre-existing finite-difference code and a new finite-element code developed using a new finite-element flux-corrected transport (FE-FCT) method. The finite-element results are shown to be almost identical to the finite-difference results. The finite-element method, however, through the use of unstructured grids, reduces significantly the number of unknowns and makes the modelling of streamers and arbitrarily shaped electrodes in two dimensions a feasible task.

1. Introduction

To date, streamer calculations have generally been carried out for gaps of 2–5 cm [18] with 20 kV applied between the electrodes. However, there are many applications in which breakdown occurs in smaller gaps (of the order of millimetres) at lower voltages (2–5 kV), such as contact breaker points and the corona treatment of plastics [2, 3, 10]. In this paper, such short gaps are considered using the same finite-difference code as that which was used successfully for larger gaps [18], as well as a new finite-element code developed for gas-discharge calculations [8]. By using the new finite-element method, unstructured grids can be used, which reduce significantly the number of unknowns for the same problem, compared with the finite-difference (FD) structured grids; hence less computation time is required. This makes the modelling of gas-discharge problems in two dimensions, which has been prohibitively time consuming up to now, a feasible task and allows the modelling of arbitrarily shaped electrodes.

Numerical results are obtained for a roughly $\sim 50 \mu\text{m}$ radius point, 1 mm from a plane in air at atmospheric pressure, with a positive voltage applied to the point. The finite-difference method, which had previously been used for 2–5 cm gaps with a 0.5 mm point, is used to compute the formation of streamers in this short 1 mm gap.

A crucial factor in the success of the finite-difference code has been the use of a very accurate flux-corrected transport (FCT) algorithm to describe the movement of electrons and ions, with no numerical diffusion or spurious oscillations and negative density values. Accordingly, a new finite-element code, using once again the FCT technique, was developed [8] and coupled with a finite-element solution of Poisson's equation, to produce a new gas-discharge code capable of describing streamer formation.

In order to test and verify the finite-element code, the same calculations as those for 1 mm gap with an applied voltage of 3 kV are repeated using the finite-element code and the results are compared with the finite-difference results. (Seldom is it possible to compare the results from such

radically different codes under identical conditions, due to the large number of calculations involved.)

The finite-element method is finally used to study the effects of the channel radius and applied voltage on the streamer speed, maximum field and current output for the 1 mm point–plane gap.

2. Theory

Complete characterization of streamer phenomena would require the use of two-dimensional models. However, due to the fact that very long calculations are employed for such problems, together with the fact that streamers occupy a narrow cylindrical channel between the anode and the cathode [14], a fixed channel radius is assumed and the equations for charges are solved in one dimension only. The electrical field must, nevertheless, be computed in two dimensions by solving Poisson's equation. So the electron, positive-ion and negative-ion continuity equations including ionization, attachment, recombination and photo-ionization are solved simultaneously with Poisson's equation, but in one dimension, to give electron and ion density distributions and the electrical field.

The coupled continuity equations for electrons, positive ions and negative ions are:

$$\frac{\partial N_e}{\partial t} = S + N_e \alpha |W_e| - N_e \eta |W_e| - N_e N_p \beta - \frac{\partial(N_e W_e)}{\partial z} + \frac{\partial}{\partial z} \left(D \frac{\partial N_e}{\partial z} \right) \quad (1)$$

$$\frac{\partial N_p}{\partial t} = S + N_e \alpha |W_e| - N_e N_p \beta - N_n N_p \beta - \frac{\partial(N_p W_p)}{\partial z} \quad (2)$$

$$\frac{\partial N_n}{\partial t} = N_e \eta |W_e| - N_n N_p \beta - \frac{\partial(N_n W_n)}{\partial z} \quad (3)$$

where t is the time, z is the distance from the cathode, N_e , N_p and N_n are the electron, positive-ion and negative-ion densities, respectively, and W_e , W_p and W_n are the electron, positive-ion and negative-ion drift velocities, respectively. The symbols α , η , β and D denote the ionization, attachment, recombination and electron-diffusion coefficients, respectively. The term S is the source term due to photo-ionization [18]. The recombination coefficients β_{ep} and β_{np} are taken to be constant and equal to β following Morrow and Lowke [18], for recombination is not an important process on the time scales involved for short point–plane gaps.

Poisson's equation is given by

$$\nabla(\epsilon_r \nabla \phi) + \frac{e}{\epsilon_0} (N_p - N_n - N_e) = 0 \quad (4)$$

where ϵ_0 is the dielectric constant of free space, ϵ_r the relative permittivity, e the electron charge and ϕ the electrical potential. The electrical field E is computed using

$$E = -\nabla \phi. \quad (5)$$

It is assumed that the transport properties of the gas (such as α and W_e) are determined by the ratio E/N , where E is the local electrical field and N is the neutral gas number

density. This assumption is valid only for high pressures [16]. The actual expressions fitted to the material data functions are tabulated elsewhere [18, 20].

The continuity equation for electrons, equation (1), is of second order and therefore requires two boundary conditions: at the anode $z = 0.1$ cm and $N_e = 0$ and at the cathode $z = 0$ and $N_e = 0$. The continuity equations for positive and negative ions, equations (2) and (3), are both of first order and thus require only one boundary condition each: at the cathode $N_n = 0$ and at the anode $N_p = 0$. At absorbing boundaries, the heavy-particle densities are finite and determined by the flux from the body of the discharge. The current, I , in the external circuit, due to the motion of electrons and ions between the electrodes, is calculated using Sato's equation [24] which is modified to include negative ions and electron diffusion:

$$I = \frac{Ae}{V_a} \int_0^d \left(N_p W_p - N_n W_n - N_e W_e + D \frac{\partial(N_e)}{\partial z} \right) E_l dz \quad (6)$$

where V_a is the applied voltage, A the cross sectional area of the discharge channel, d the gap length and E_l the Laplacian electrical field.

Poisson's equation is solved on a two-dimensional mesh with boundary conditions $\phi = \phi_0$ (the applied voltage) at the anode surface, $\phi = 0$ at the cathode and $\partial\phi/\partial r = 0$ along the axis of symmetry. At the open boundary, the charge is assumed to be zero, so the exact solution of Laplace's equation is used [7, 12].

3. Solution methods

Much work has been done on the development of models for streamer problems in one dimension by using the same set of equations [9, 19, 26]. It is worth noting, however, that all these models are limited to structured grids (for the two-dimensional solution of Poisson's equation). It is clear that the extension of these models in fully two-dimensional form would result in very long calculations due to the fact that, when one is using structured grids, many unknowns are required, especially for gas-discharge problems, in which a very fine resolution is required for certain parts of the space domain (such as the anode). There are also fully two-dimensional finite-difference models [1, 6, 11, 28], again using structured grids, but these are limited to small gaps or small time domains due to the computational expense of the calculations.

The problem presented in this paper is solved using one of these finite-difference models, developed by Steinle *et al* [26], and the new finite-element method, developed by the authors [8], to demonstrate the advantages of the finite-element unstructured grids over the finite-difference structured grids. This also acts as a good validation of this code before extending it to two dimensions. The inputs for the two codes are the same so that they act as a detailed check on each other.

The finite-difference method uses a successive over-relaxation method [23] to obtain the two-dimensional axisymmetrical solution of the electric potential ϕ from Poisson's equation. The continuity equations are solved

using a very accurate fourth-order flux-corrected transport algorithm [26].

The second method uses a new finite-element algorithm recently developed by the authors [8], which uses the standard Taylor–Galerkin method for the solution of Poisson’s equation, together with a new improved finite-element flux-corrected transport (FE-FCT) algorithm for the continuity equations. This improved FE-FCT algorithm is an extension of the method proposed by Lohner *et al* [13], which has been used very successfully in fluid mechanics and has the distinct advantage that no operation splitting for multidimensional problems is required. The two-step Lax–Wendroff method is used as the high-order scheme and mass diffusion is added to transform this high-order scheme to a low-order one. Diffusion is added by subtracting the lumped mass matrix from the consistent mass matrix and the diffusion coefficient used is the one inherent in the upwind scheme. This is the optimal diffusion coefficient for the performance of the FCT algorithm. More details can be found in [8].

For fast-moving transient phenomena, such as streamer fronts, a moving mesh is usually required. However, the continuous movement of the mesh is inappropriate for this calculation. Firstly, many geometrical parameters would have to be recalculated at every time step, making the computation inefficient. Secondly, the electrons move in the opposite direction to that of the streamer front, increasing the effective value of W_e relative to the mesh and reducing the value of the time increment required for numerical stability.

The strategy adopted for both the methods (finite difference and finite elements), in order to follow the streamer front, has been to use a fine uniform mesh, across which the streamer head propagates, and an expanding mesh away from this region towards the electrodes. When the streamer reaches the end of the fine mesh region, the mesh is re-zoned so that the streamer head is again at the start of the fine mesh region.

At the anode, a fine mesh is also used to resolve the anode-fall region. The mesh expands smoothly away from the anode and then contracts towards the streamer-head region. Similarly the mesh expands away from the streamer-head region towards the cathode, but with no fine mesh region at the cathode. The smooth changes and expansion of the mesh are achieved using exponential functions. The total number of axial mesh points used to represent the 1 mm gap between the cathode and the anode both for the finite-difference method and for the finite-element method is 400. The mesh size at the streamer head is $2 \mu\text{m}$. The continuity equations are solved on this mesh of 400 points.

Poisson’s equation is solved on a two-dimensional mesh. For the finite-difference method, radial dimensions have to be defined and further axial dimensions have to be defined so that the shape of the anode is included. The radial mesh has a minimum size of $5 \mu\text{m}$ at the centre, expanding exponentially with 50 mesh points out to a radius of 1 mm. The shape of the anode is included by defining a new axial mesh point for each radial mesh point such that the position defined by the axial and radial coordinates lies on the anode surface. In this way, the anode is included using an extra 40 mesh points. Thus, for the finite-difference method, Poisson’s equation is solved on a mesh of 440 axial points and 50 radial points, which

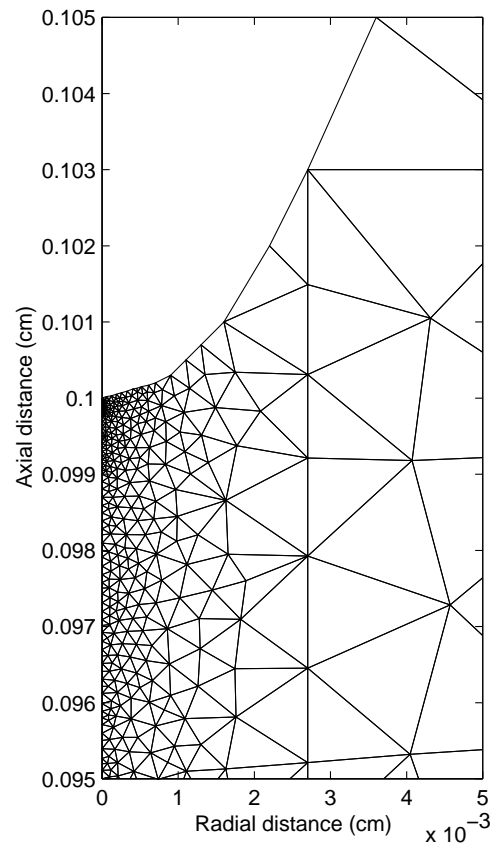


Figure 1. The high-resolution mesh at the anode region for the finite-element solution of Poisson’s equation.

results in about 20 000 unknowns. Furthermore, for the finite-difference method, Poisson’s equation is solved using the successive over-relaxation (SOR) method [23] which takes up to 50 iterations at each time step and hence dominates the computation time of the whole problem.

On the other hand, with the finite-element method, unstructured grids are used, through the use of triangular elements, which reduce the number of unknowns significantly for the same problem and allow one to model the boundaries more accurately. Figure 1 shows the anode region of the mesh used for the solution of Poisson’s equation using the finite-element method. It is clearly seen that a very fine resolution is used in the anode region to resolve the steep gradients, as required, but, away from the axis of symmetry, where the space charge is zero, a very coarse mesh is used because the solution there does not vary steeply. The total number of unknowns used for the solution of Poisson’s equation is now around 4000. In this way, the accuracy is maintained at less computational expense, compared with the finite-difference method, in which structured grids must be used and the boundaries are represented more accurately, which allows us to model arbitrarily shaped electrodes.

Furthermore, with the finite-element method, the problem reduces to solving the following equation after discretization:

$$\mathbf{M}\phi = \mathbf{q} \quad (7)$$

which gives

$$\phi = \mathbf{M}^{-1}\mathbf{q} \quad (8)$$

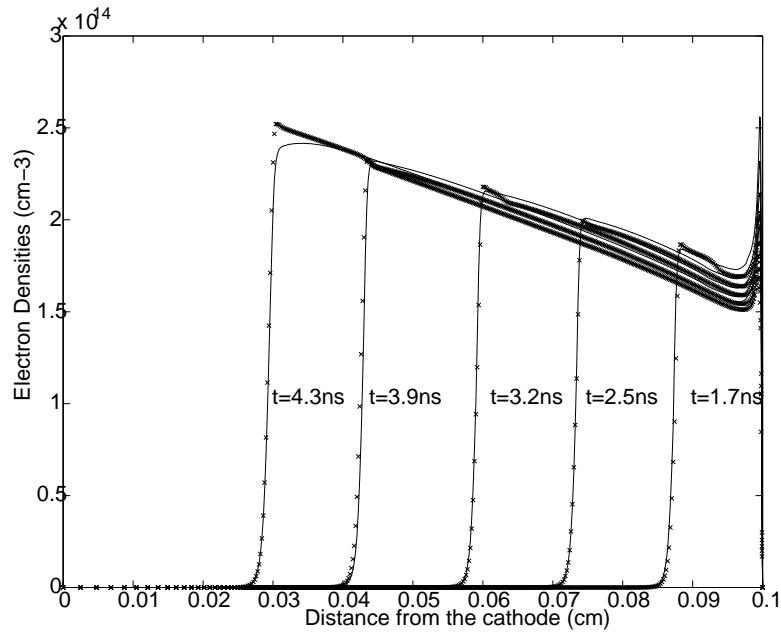


Figure 2. Electron densities at various times: full line, finite-difference results; and (\times), finite-element results.

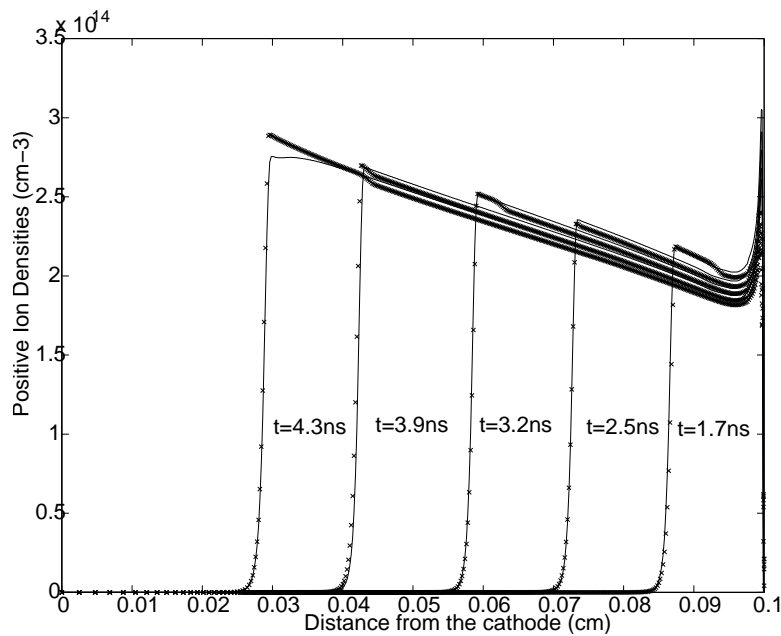


Figure 3. Positive-ion densities at various times: full line, finite-difference results; and (\times), finite-element results.

where \mathbf{M} is a global matrix associated with the finite-element method [25], assembled by the elemental matrices, ϕ the vector of unknown electrical potential values at each node and \mathbf{q} the vector of charges, obtained from the continuity equations, at each node. For this problem, the matrix \mathbf{M} is constant for a constant mesh, for it depends only on the voltage and the mesh, so it can be inverted at the beginning of the calculation and stored. Thus, the 50 iterations for each time step of a problem of 20 000 unknowns (the finite-difference case) reduce to a single matrix-vector multiplication of 4000 unknowns (the finite-element case) and hence the computational effort is reduced significantly.

4. Results

Results are presented for the development of streamers from the positive point of a point-plane gap in air at atmospheric pressure. The point is a hyperboloid with a $50 \mu\text{m}$ radius of curvature at the tip, the gap spacing is 1 mm and a positive voltage is applied at the start of the calculation. The calculations refer to the situation in which there is no pre-existing space charge and the voltage can reach a steady state before the discharge starts, as was the case for the original Trichel pulse calculation of [15]. Experimentally there is often a long time lag before a suitable seed electron is available to start the discharge, during which time the

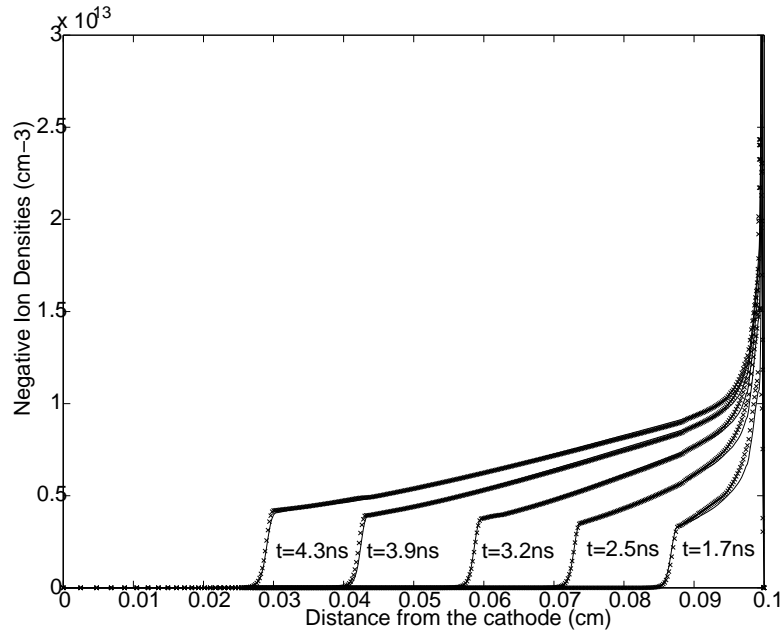


Figure 4. Negative-ion densities at various times: full line, finite-difference results; and (x), finite-element results.

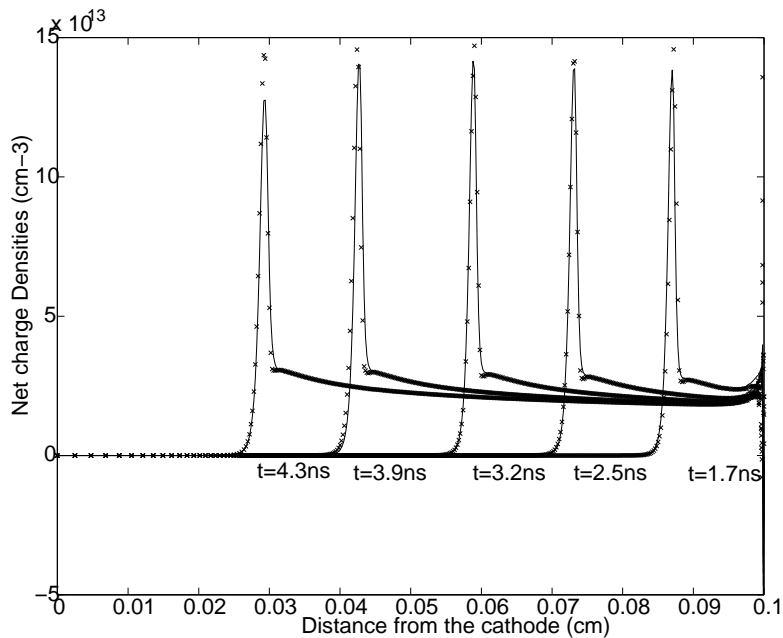


Figure 5. The net charge at various times: full line, finite-difference results; and (x), finite-element results.

voltage reaches a steady state. Subsequent discharges are considerably affected by the existence of space charge, just like the case for Trichel pulses, for which subsequent pulses are smaller than the first [4]. In this paper we consider only the first corona phenomena.

4.1. A FE–FD comparison

In order to test and verify the finite-element method, a streamer calculation is performed both with both the finite-element code and with the finite-difference code, with exactly the same inputs. For this test a voltage of 3 kV is applied to the point at the start of the calculation and the calculation

is initiated by approximately 100 electron ion pairs released 0.2 mm from the anode at $t = 0$. The radial charge density is distributed radially using

$$\rho(r, z) = \rho_a(z) e^{-100r^2} \tag{9}$$

where $\rho_a(z)$ is the axial charge distribution. The charge is set out up to a distance of 0.0075 cm and is set to zero beyond this point for this problem. This choice of radial distribution is imposed on the calculation in order to make the results directly comparable with those published previously [18] and in order to use exactly the same program as that used in [18] for the validation of the finite-element program. The effects

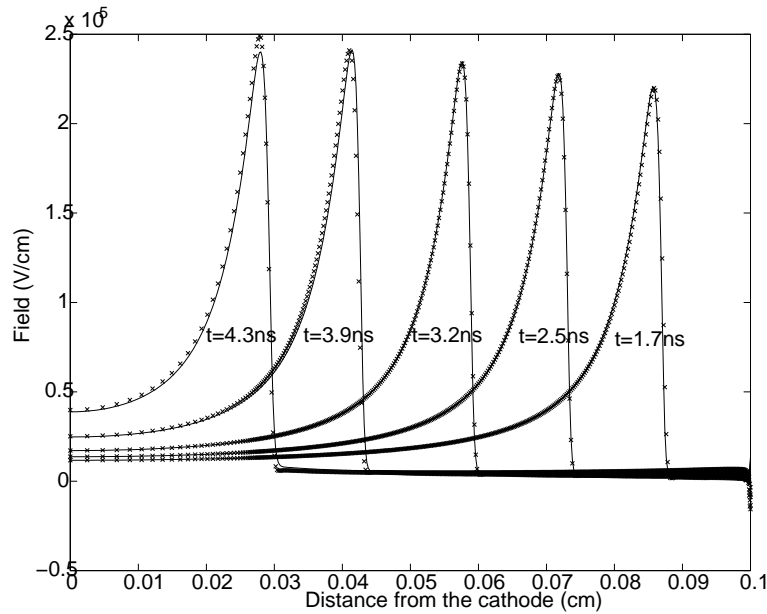


Figure 6. The field along the axis of symmetry at various times: full line, finite-difference results; and (\times), finite-element results.

of changing the radial dimensions and the radial profile to a square profile are discussed in a later section.

Figures 2–6 show the electron, positive-ion, negative-ion and net charge densities and the field along the axis of symmetry, respectively, at various times during the movement of the streamer towards the cathode. Figures 7 and 8 show the field obtained in the whole of the space domain from the solution of Poisson's equation at times $t = 1.7$ and 3.2 ns. The results obtained with the two methods are shown to be in good agreement and this gives us confidence that the finite-element method gives comparable results at less computational expense than the finite-difference method for the solution of streamer problems. Thus the finite-element method is used in the subsequent sections for the analysis of the case of a 1 mm point–plane gap.

4.2. The radial charge distribution

It is a weakness of the present approach that a radial profile must be specified; however, such methods are much more efficient than two-dimensional methods and give comparable results to those for two-dimensional methods, provided that a suitable radius is chosen for the channel [1, 11]. It is not appropriate to compute a suitable streamer radius by considering the radial expansion of an electron avalanche, due to diffusion, as it grows large enough to distort the electric field [4]. This is because we are considering not a single avalanche but many avalanches which are rapidly absorbed into the anode. Our best guide is to draw the right streamer radius from the existing literature on two-dimensional modelling of streamers.

The early two-dimensional modelling of Dhali and Williams [5] indicated that streamers could propagate at various radii depending on the initial electron distribution. However, the recent results of Vitello *et al* [27] show that changing the initial radius of the electron distribution by a factor of two changes the initial stages of the streamer development, but

then the streamer reverts to propagating with the same diameter of about $100 \mu\text{m}$, which is similar to that found by Wang and Kunhardt [29] and Babaeva and Naidis [1]. Whereas Vitello *et al* find their streamer propagating with a relatively constant radius, Kulikovski [11] computes a streamer whose diameter varies from 40 to $300 \mu\text{m}$ as the streamer traverses a 1 cm gap. Thus the question of the appropriate streamer diameter to use is not well answered at present, but the order of magnitude is clearly about $100 \mu\text{m}$.

The Gaussian radial density distribution used in [18] is used in this paper; however, results of using different radial distributions are presented, including that for a square distribution, with a uniform density up to a fixed radius, which may be closer to the two-dimensional results. The Gaussian radial density distribution considered here is of the form

$$\rho(r, z) = \rho_a(z) e^{-(r/r_0)^2} \quad (10)$$

where $\rho_a(z)$ is the axial density distribution and r_0 is the channel radius. The first calculations were obtained using a 3 kV voltage and varying the channel radius. A Gaussian profile of 10^6 cm^{-3} electron–ion pairs centred 0.095 cm from the cathode with a half-width of 0.001 cm was used as the initial charge distribution.

Figure 9 shows the variation of the electric field at the streamer head (E_{max}) with the channel radius. E_{max} depends weakly on external conditions and, for all variants of two-dimensional modelling of streamers at atmospheric air, this is in the range 150 – 180 kV cm^{-1} [1]. So the appropriate channel radius can be chosen to satisfy this requirement; for an applied voltage of 3 kV this radius is about 0.01 cm. The streamer calculation is then repeated for 0.01 cm channel radius. Figures 10, 11, 12 and 13 show the electron, positive-ion, negative-ion and net charge densities, respectively, at various instants during the streamer development. The electron density is found to be in the range $(1$ – $1.4) \times 10^{14} \text{ cm}^{-3}$ which agrees with the previously

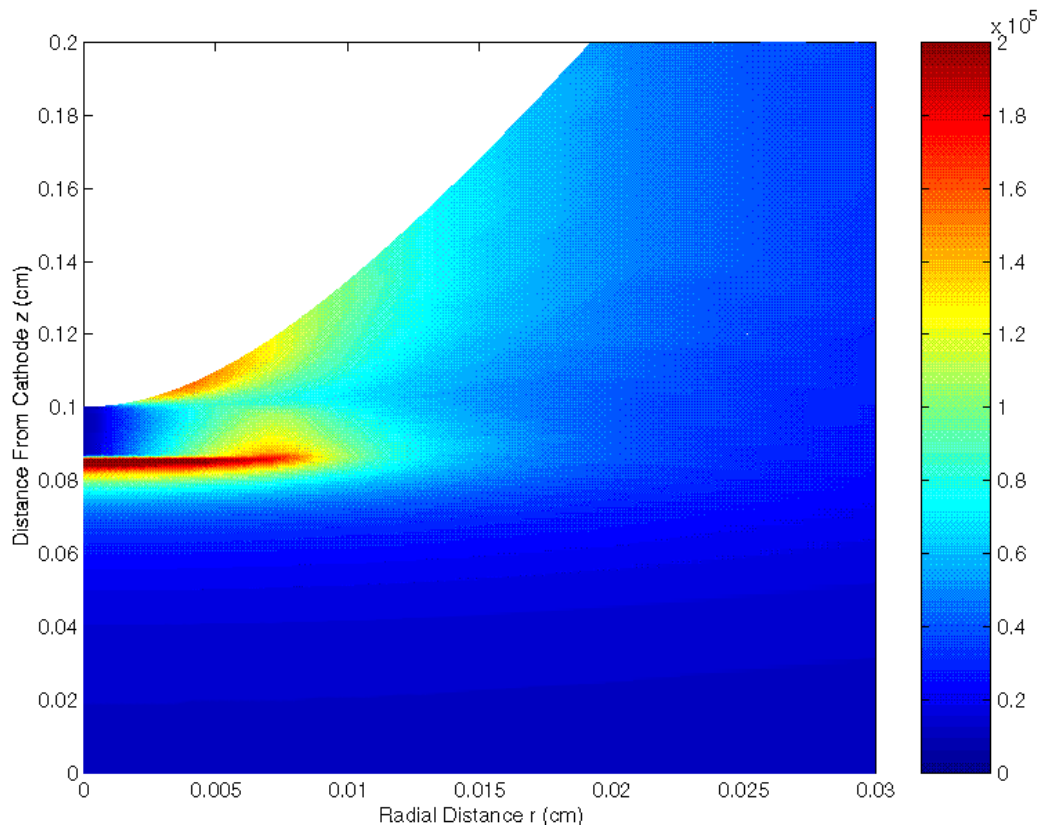


Figure 7. The field distribution in the whole of the space domain obtained from the solution of Poisson's equation at time $t = 1.7$ ns using the finite-element method.

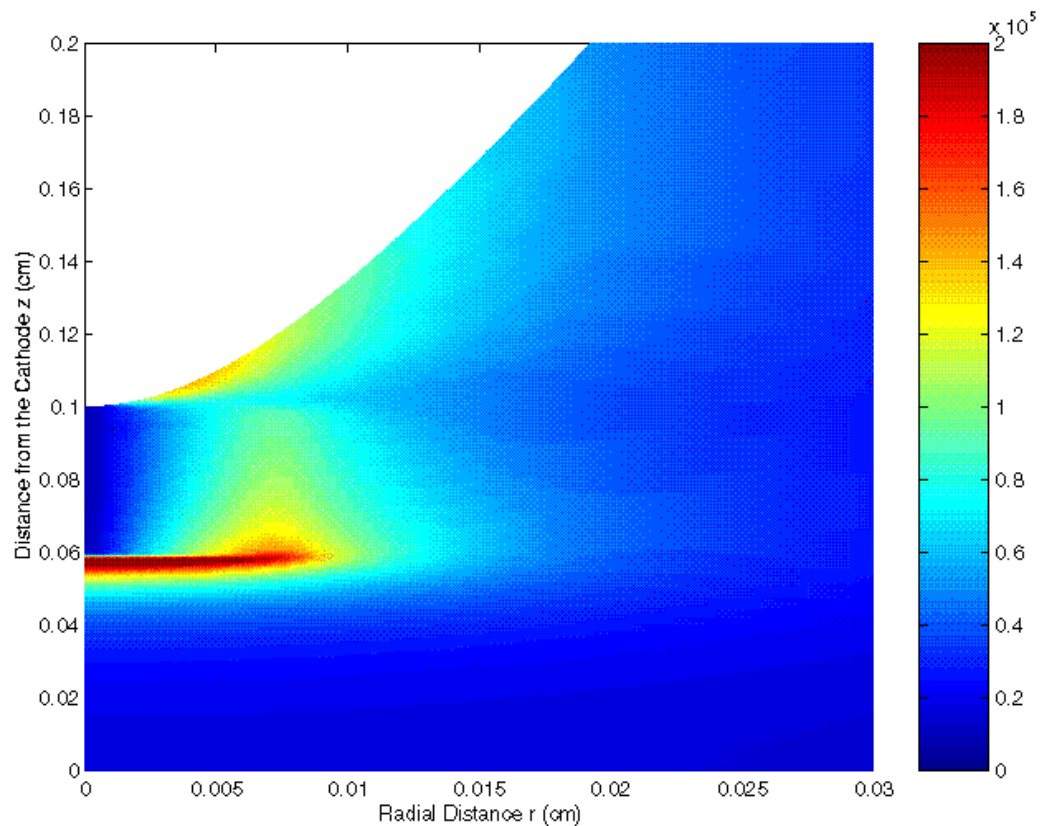


Figure 8. The field distribution in the whole of the space domain obtained from the solution of Poisson's equation at time $t = 3.2$ ns using the finite-element method.

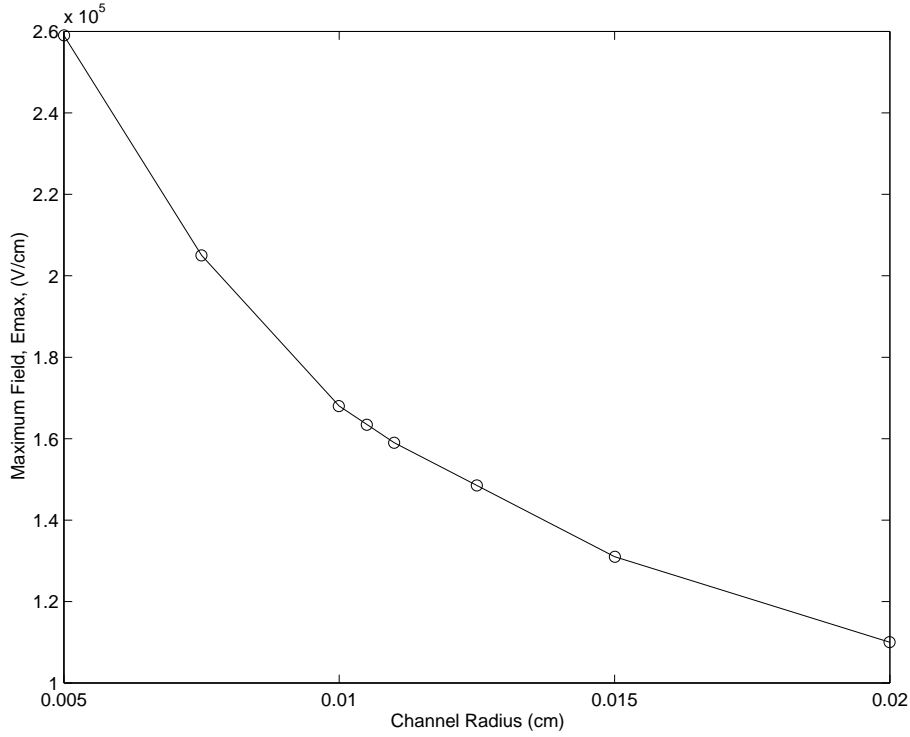


Figure 9. The variation of the maximum streamer field (E_{max}) with the channel radius.

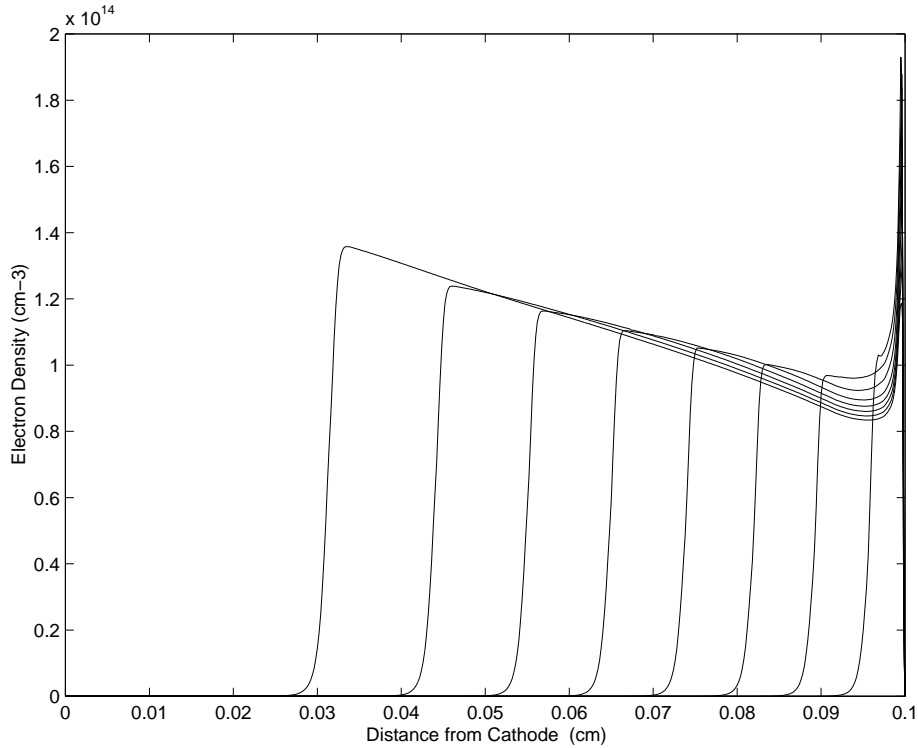


Figure 10. Electron densities at 3 kV with a channel radius of 0.01 cm and a Gaussian radial distribution. The instants shown are (from left to right): 1.42, 2.03, 2.64, 3.22, 3.80, 4.35, 4.88 and 5.39 ns.

published two-dimensional numerical results [1]. Figure 14 shows the electric field distribution at various instants and the maximum field is found to be in the range 160–180 kV cm⁻¹. Finally, figure 15 shows the field behind the streamer head at several instants. A point worth noting is the very low field

obtained during the early stages of the streamer development. For a short gap and a very sharp point such as the 1 mm gap and 50 μm radius tip, the field at the surface is very high. Thus substantial ionization is taking place and electrons are flooding back to the anode at the start of the discharge;

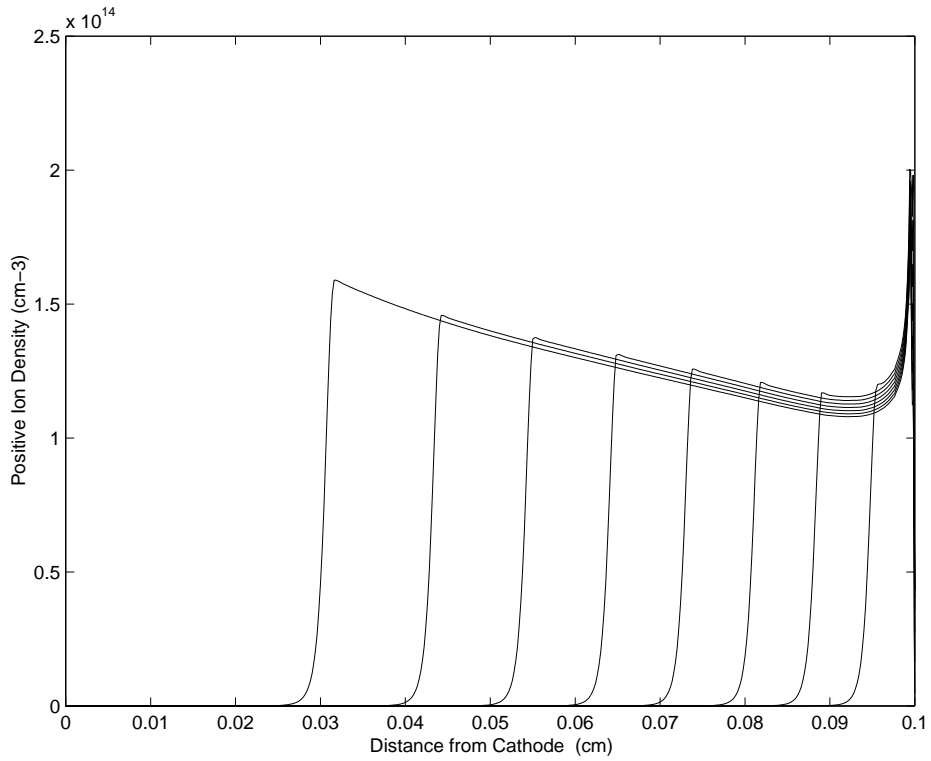


Figure 11. Positive-ion densities at 3 kV with a channel radius of 0.01 cm and a Gaussian radial distribution. The instants shown are (from left to right): 1.42, 2.03, 2.64, 3.22, 3.80, 4.35, 4.88 and 5.39 ns.

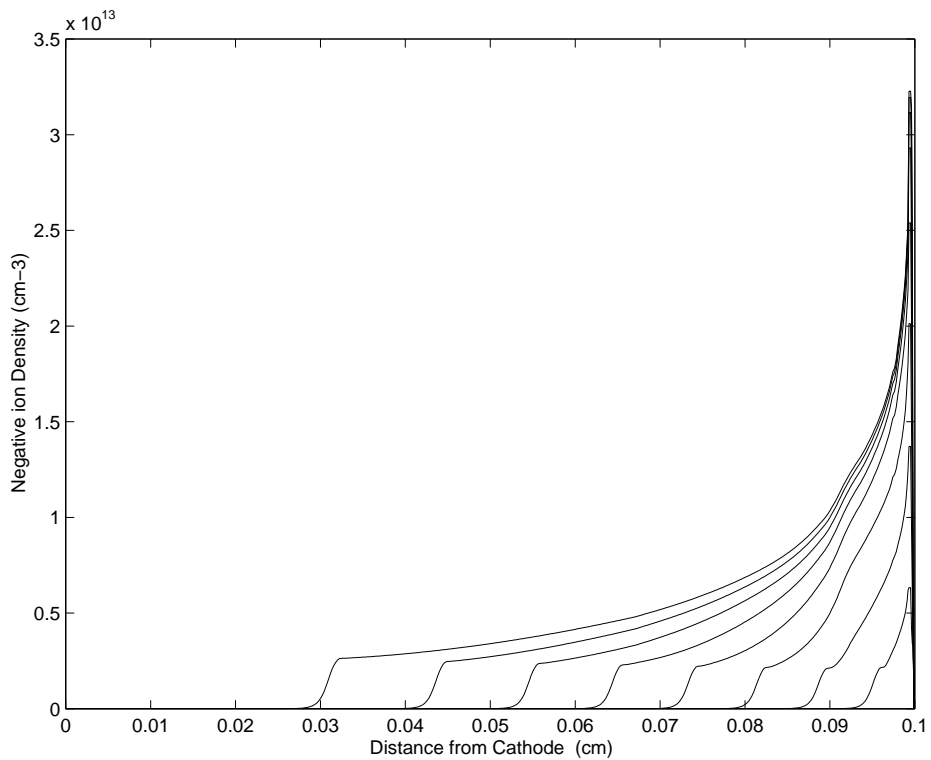


Figure 12. Negative-ion densities at 3 kV with a channel radius of 0.01 cm and a Gaussian radial distribution. The instants shown are (from left to right): 1.42, 2.03, 2.64, 3.22, 3.80, 4.35, 4.88 and 5.39 ns.

consequently there need only be a low field to maintain the current in the channel left over from the earlier stages, by the streamer head. Also attachment is very slow; hence electrons

are not lost and thus a high field is not necessary to maintain the current by conduction or by ionization to create more current carriers. That is why, during the early stages of the

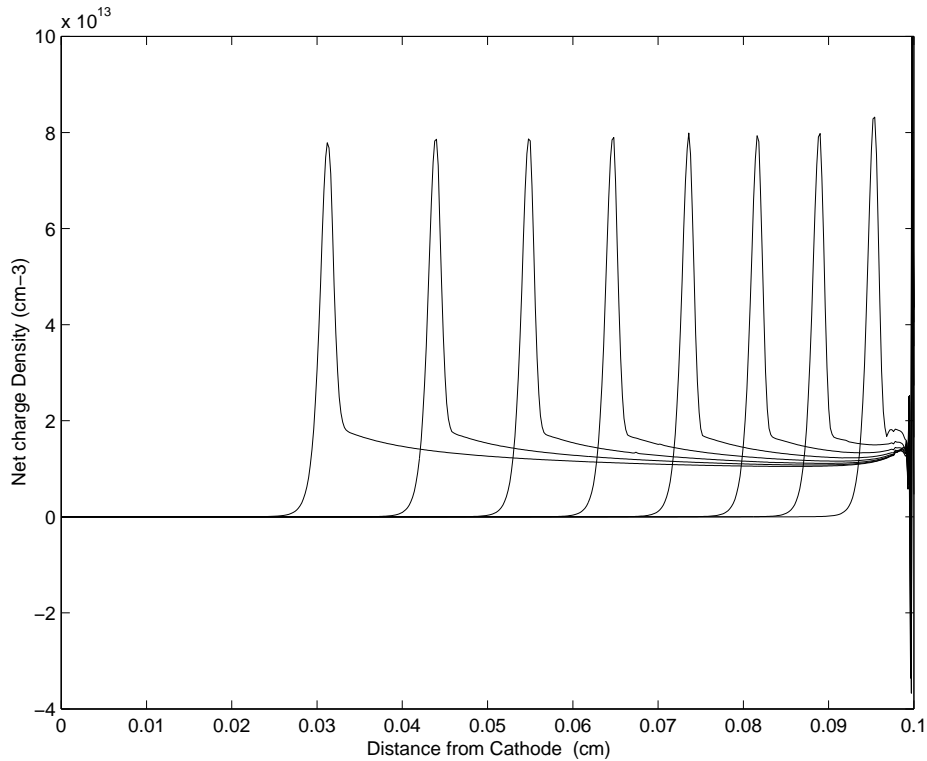


Figure 13. Net charge densities at 3 kV with a channel radius of 0.01 cm and a Gaussian radial distribution. The instants shown are (from left to right): 1.42, 2.03, 2.64, 3.22, 3.80, 4.35, 4.88 and 5.39 ns.

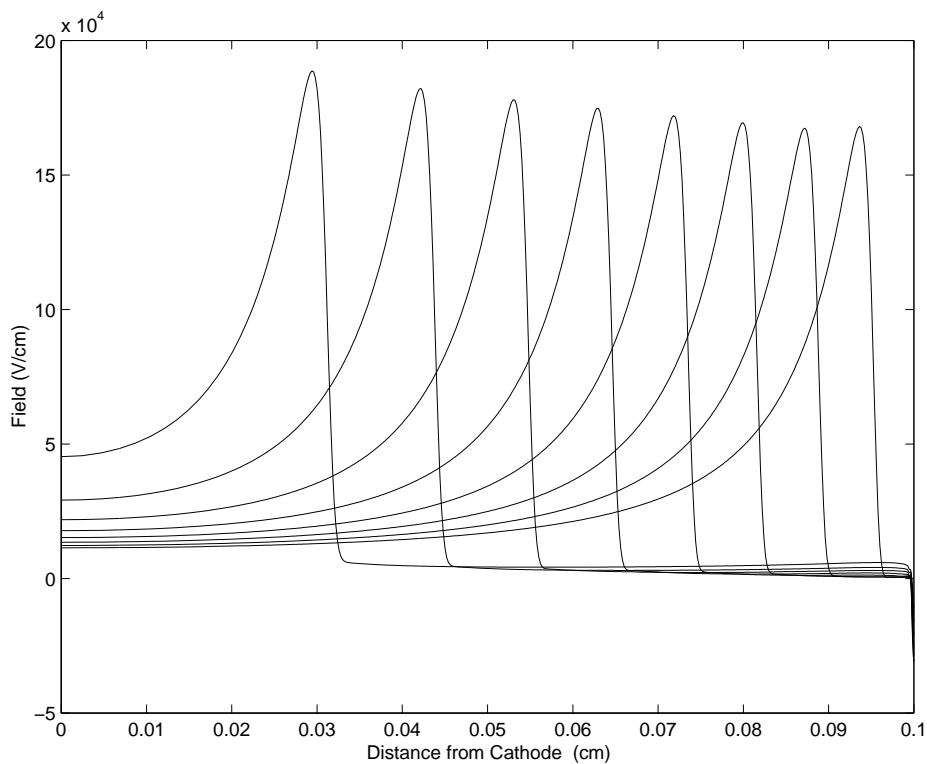


Figure 14. The field along the axis of symmetry at 3 kV with a channel radius of 0.01 cm and a Gaussian radial distribution. The instants shown are (from left to right): 1.42, 2.03, 2.64, 3.22, 3.80, 4.35, 4.88 and 5.39 ns.

streamer development, the field behind the streamer in the small gap is much smaller than what is predicted for wider gaps ($6\text{--}8\text{ kV cm}^{-1}$) [1]. As the streamer advances towards

the cathode, the field in the streamer head rises and most of the electrical energy is concentrated between the streamer head and the cathode. Thus ionization occurs more rapidly

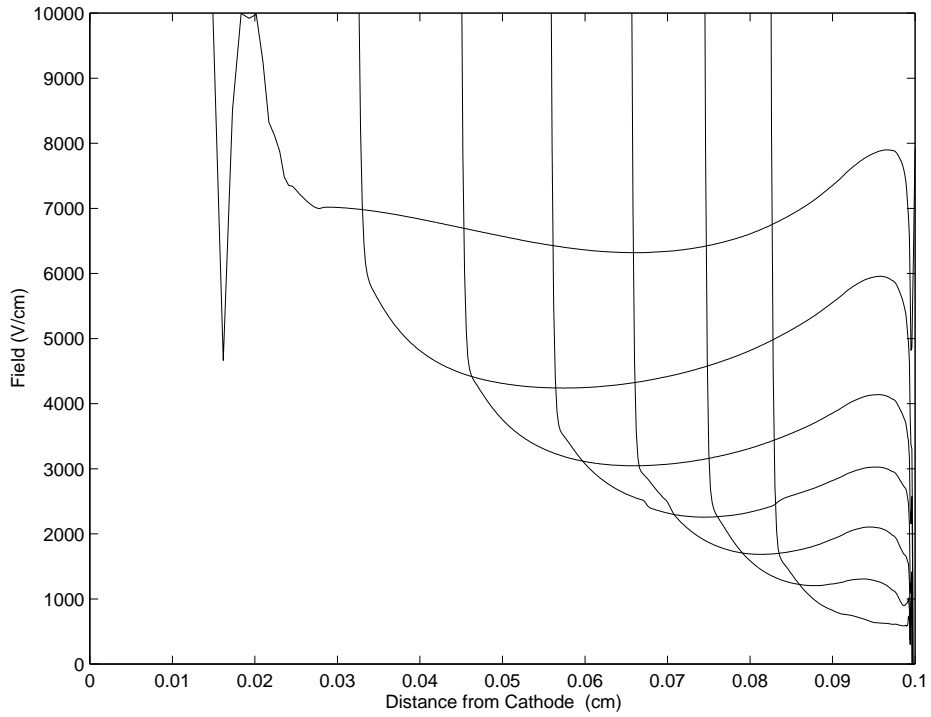


Figure 15. The field behind the streamer head at 3 kV with a channel radius of 0.01 cm and a Gaussian radial distribution. The instants shown are (from left to right): 2.64, 3.22, 3.80, 4.35, 4.88, 5.39 and 5.87 ns.

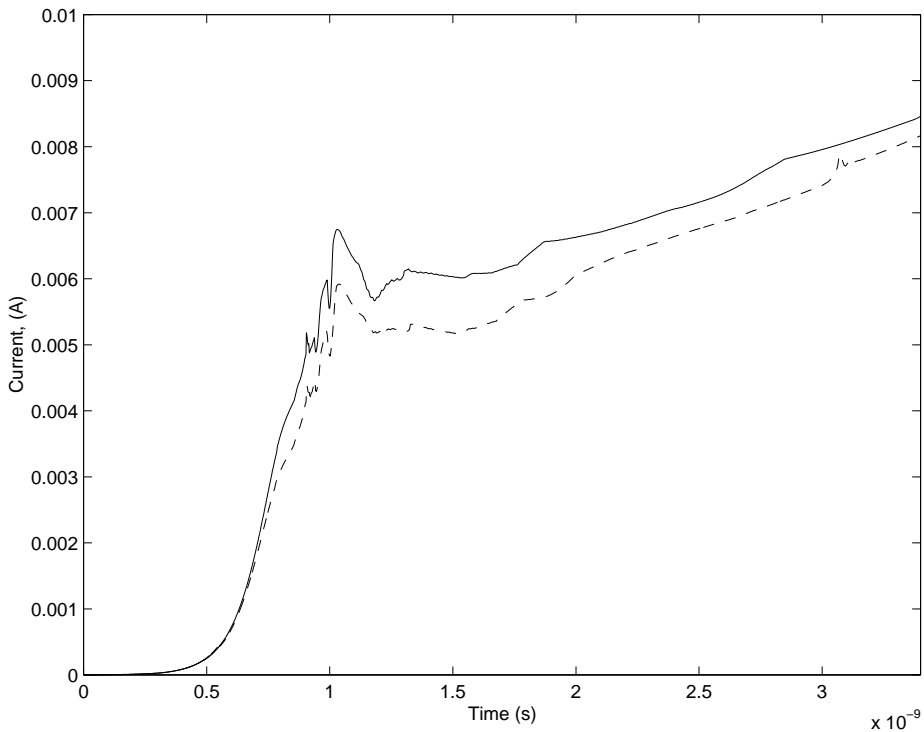


Figure 16. The external circuit current at 3 kV with a channel radius of 0.01 cm: full line; a Gaussian radial charge distribution; and broken line, a constant radial charge distribution.

over a wider region and the current rises very rapidly. At the same time attachment is removing electrons from the channel and the field behind the channel rises steadily to values up to about 7 kV cm^{-1} (see figure 15), which agrees with the two-dimensional predictions ($6\text{--}8 \text{ kV cm}^{-1}$).

The same calculation is repeated, but this time with a constant radial distribution and a channel radius of 0.01 cm with an applied voltage of again 3 kV. The results were found to be very similar to the results obtained with the Gaussian profile of 0.01 cm channel radius. Figure 16 shows the

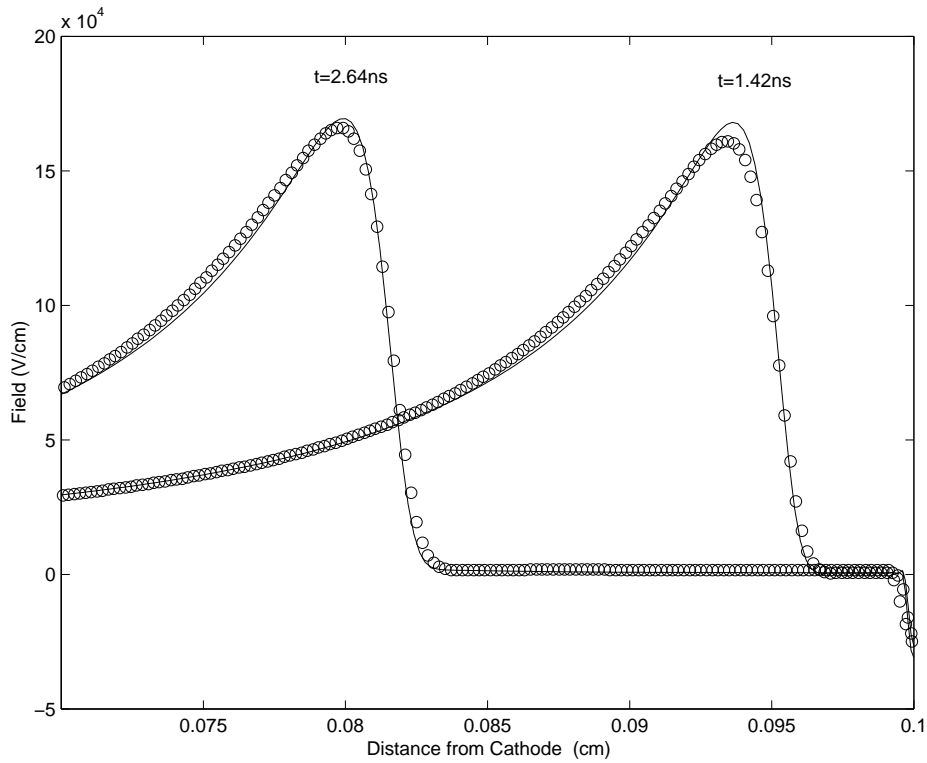


Figure 17. The field along the axis of symmetry at 1.42 and 2.64 ns with an applied voltage of 3 kV and a streamer radius of 0.01 cm: full line, a Gaussian radial charge distribution; and (o), a constant radial charge distribution.

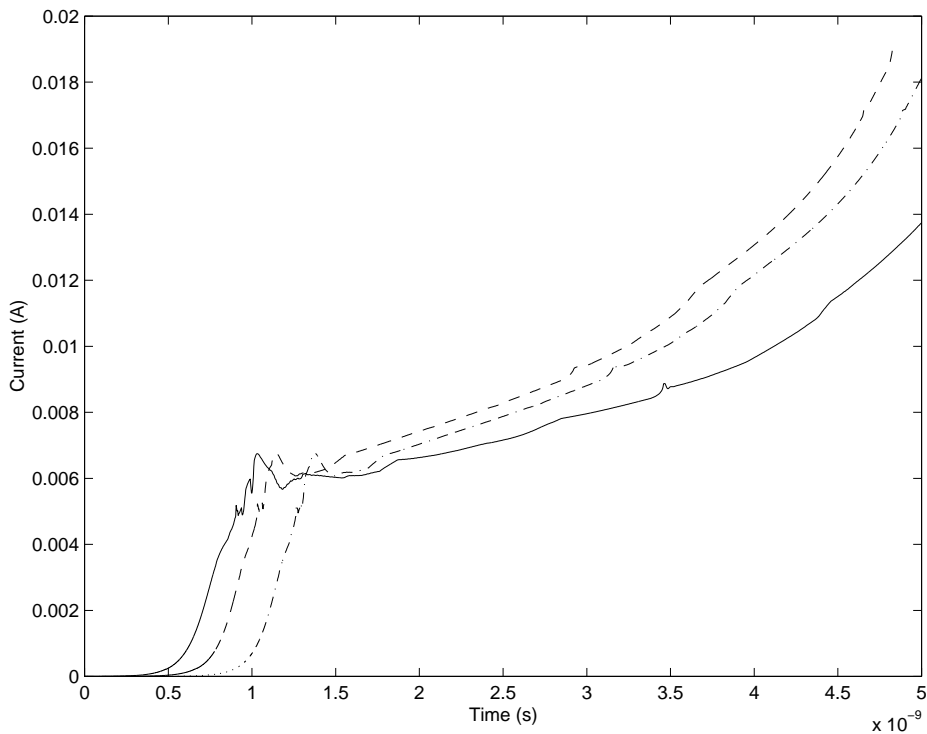


Figure 18. The external circuit current at 3 kV and 0.01 cm channel radius with various initial charge distributions: full line, a square distribution centred 0.095 cm from the cathode and of width 0.002 cm; broken line, a Gaussian charge distribution centred 0.095 cm from the cathode with a half-width of 0.001 cm; and chain line, a Gaussian distribution the same as before but centred 0.085 cm from the cathode.

external circuit current with the Gaussian radial distribution and the constant radial distribution and figure 17 shows the field along the axis of symmetry at $t = 1.42$ ns and

2.64 ns. It is evident no significant change in the results is caused by using the square profile rather than the Gaussian one.

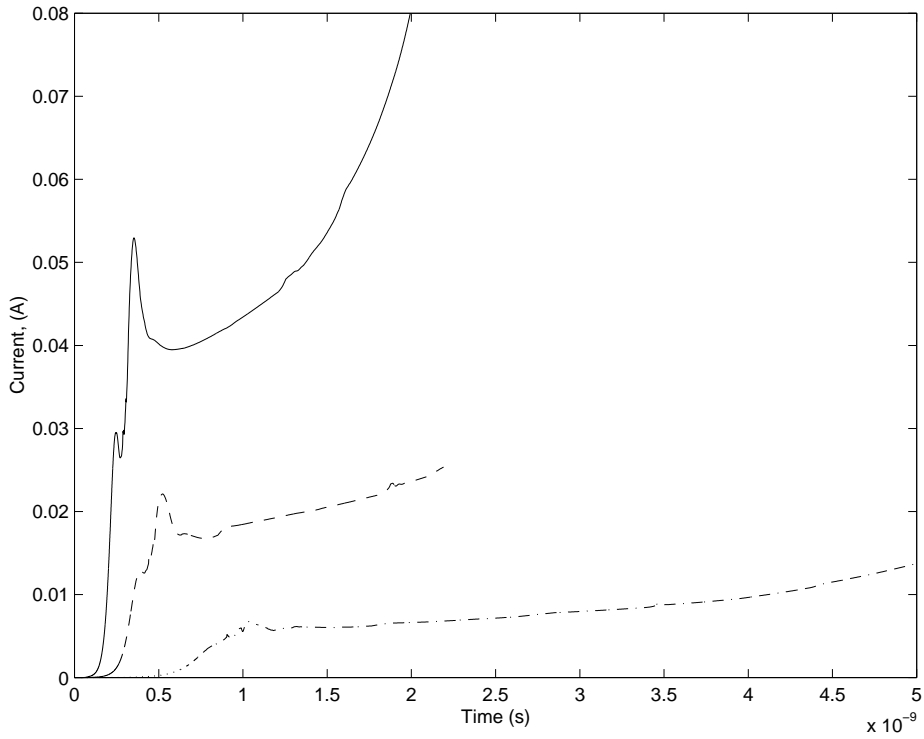


Figure 19. The external circuit current versus time at three different applied voltages: full line, 4 kV; broken line, 3.5 kV; and chain line, 3 kV.

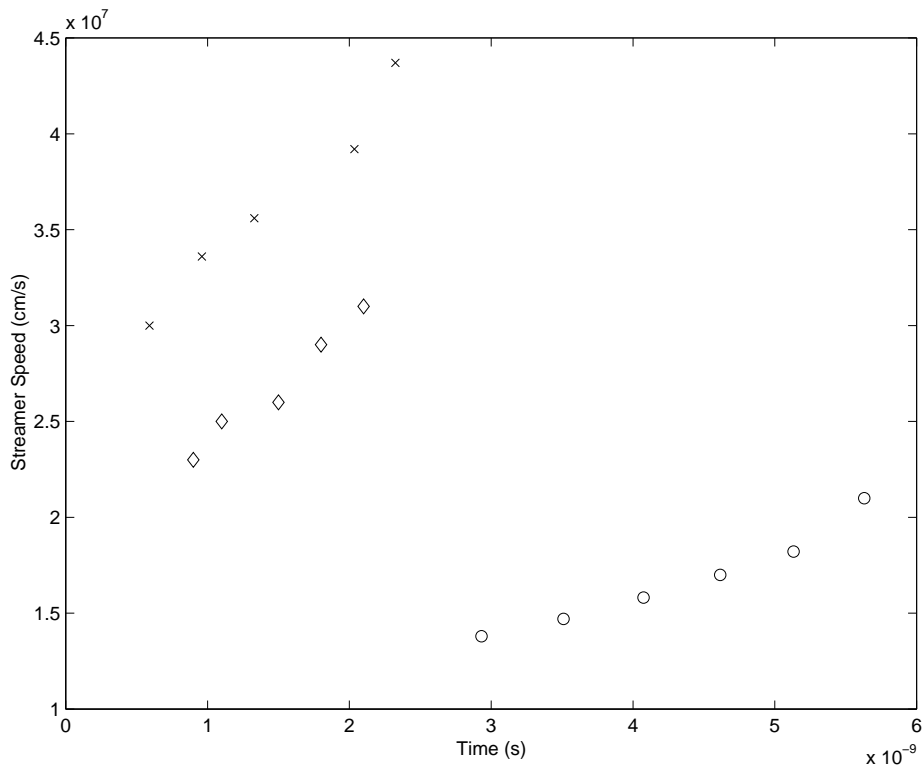


Figure 20. The streamer speed plotted against time at three different applied voltages: (o), 3 kV; (◊), 3.5 kV; and (x), 4 kV.

4.3. Initial charge profiles

The effects of various initial distributions are then examined. Figure 18 shows the current obtained using three different

initial charge distributions to initiate the calculation. The first is a square charge distribution of length 0.002 cm and amplitude 10^6 cm^{-3} centred 0.095 cm from the cathode. The second is a Gaussian pulse of amplitude 10^6 cm^{-3} and

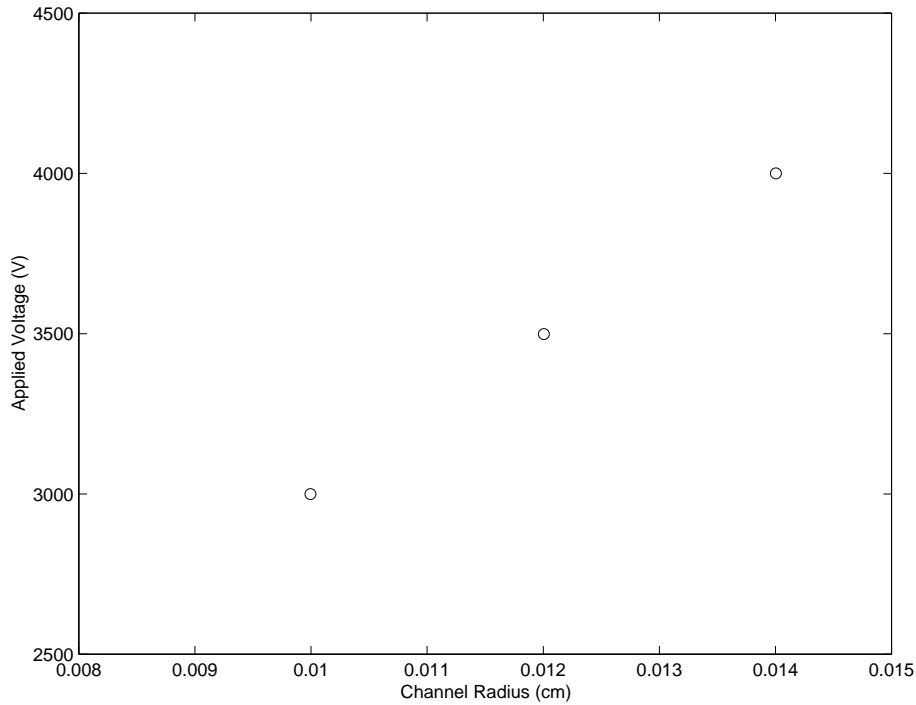


Figure 21. The streamer channel radius plotted against the applied voltage.

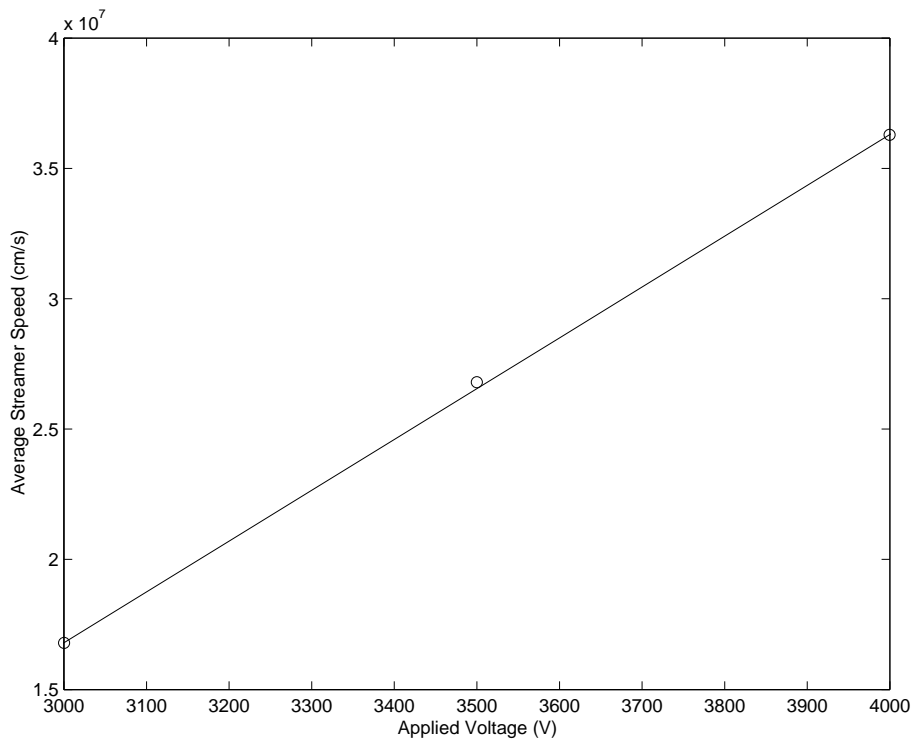


Figure 22. The average streamer speed plotted against the applied voltage.

half-width 0.001 cm centred 0.095 cm from the cathode and the third is the same Gaussian pulse as the second one but centred 0.085 cm from the cathode. The initial charge distribution does not change the characteristics of streamer propagation significantly (except near the anode) but it introduces different time delays, as shown in figure 18. Some minor oscillations in the current waveforms in the ‘dip’

following the maximum (see figure 18) are due to the lack of sufficient spatial resolution somewhere in the space domain. This kind of instability in the current has been observed previously by Morrow [17] and can be avoided by having better spatial resolution, but this clearly is unwanted, for it would make the calculation even more expensive. The observed instability, however, does not grow and this is

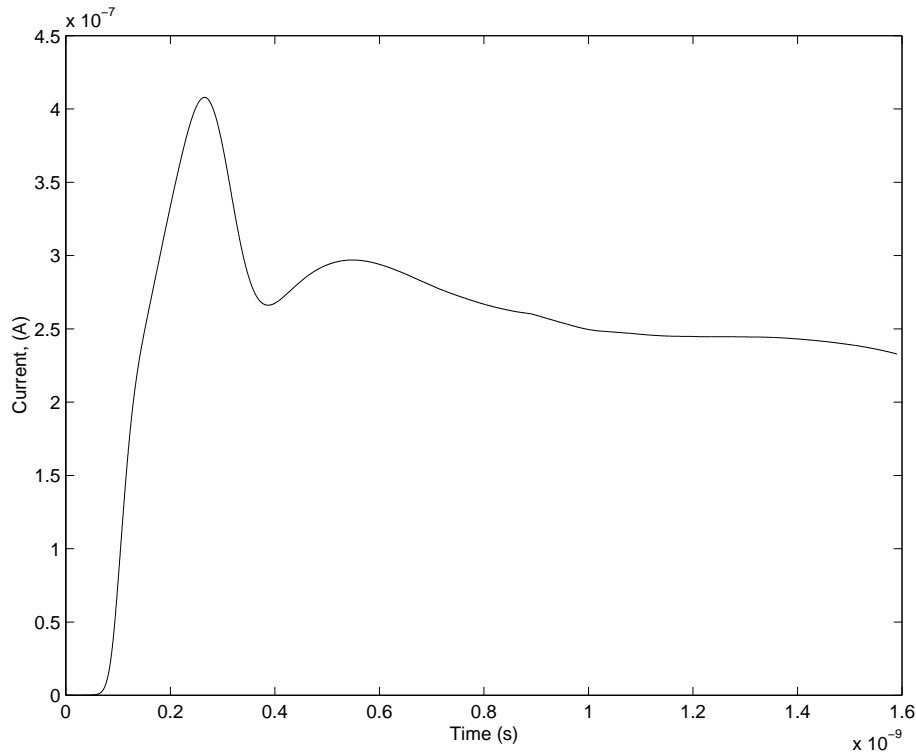


Figure 23. The external circuit current at 2.5 kV for a channel radius of 0.008 cm.

because of the use of the FCT method, which is an accurate and very robust method, for the solution of the continuity equations.

4.4. Voltage variation

The applied voltage was then varied and its effects on the streamer speed, channel radius and current were examined. Three different applied voltages were considered: 3, 3.5 and 4 kV. For the case of 3.5 kV a channel radius of 0.012 cm gave the maximum field in the range $160\text{--}180\text{ kV cm}^{-1}$, whereas for 4 kV the channel radius was 0.014 cm. The electron densities were again found to be in the range $(1\text{--}1.5) \times 10^{14}\text{ cm}^{-3}$ for both cases.

Figure 19 shows the temporal evolution of the external circuit current with the three different applied voltages, namely 3, 3.5 and 4 kV, and figure 20 shows the streamer speed at various times during the propagation of the streamer for these three voltages. The channel radius and the average streamer speed are plotted against the applied voltage in figures 21 and 22 and it is found that the channel radius and average streamer speed increase linearly with the applied voltage. This is in agreement with the theoretical results obtained by two-dimensional simulations [1].

Finally a voltage of 2.5 kV was considered with a channel radius of 0.008 cm (extrapolated from the voltage versus channel radius curve in figure 21) and this time there was no streamer formation. Figure 23 shows the current at 2.5 kV.

5. Conclusions

In this paper, the results obtained from a pre-existing finite-difference code were compared with those obtained from a

new improved finite-element flux-corrected transport code, for a short-gap streamer calculation and they were found to be in a very good agreement. Using this new finite-element method, however, allows one to use unstructured grids which offer advantages, compared with finite-difference codes, in that arbitrarily shaped electrodes can be modelled and fewer unknowns need be used for the same problem. This in turn requires less computational time.

The numerical results predicted that no streamer formed at voltages lower than or equal to 2.5 kV and that streamers formed and bridged the gap for higher voltages. The streamer speed and channel radius were found to be linear functions of the applied voltage. Finally, the field behind the streamer was found to be relatively low during the early stages of development of the streamer propagation, which is in contrast to what has been observed for longer gaps and comparable for the latter stages of the development of the streamer.

Future work involves extending this new improved finite-element code in two dimensions. The finite-difference code would be prohibitively time consuming when extended to two dimensions, due to the large number of unknowns, but with the use of finite elements the number of unknowns is reduced significantly, which makes the modelling of streamers in two dimensions a feasible task. Work on the simulation of a negative electrical corona and an electrical corona at radio frequencies is also under way.

References

- [1] Babaeva N Y and Naidis G V 1996 Two-dimensional modelling of positive streamer dynamics in non-uniform electric fields in air *J. Phys. D: Appl. Phys.* **29** 2423–31

- [2] Bird R, Blythe A R, Briggs D and Kendall C R 1982 Electrical discharge treatment of polymeric film surfaces *Proc. 7th Int. Conf. on Gas Discharges and their Applications (London)* ed D Farish *et al* (London: Peregrinus) p 163
- [3] Visking Corporation 1952 UK patent specification 715 914
- [4] Cross J A, Morrow R and Haddad G N 1996 Negative point-plane corona in oxygen *J. Appl. Phys.* **63** 5171–4
- [5] Dhali S K and Williams P F 1987 Two-dimensional studies of streamers in gases *J. Appl. Phys.* **62** 4696–707
- [6] Djermoune D, Marode E and Segur P 1995 Two dimensional modelling of a streamer induced discharge *XXII Int. Conf. on Phenomena in Ionised Gases (Hoboken, NJ)* vol 1, ed K H Becker, W E Carr and E E Kunhardt (Hoboken, NJ: Stevens Institute of Technology) p 33
- [7] Eyring C F, Mackeown S S and Millikan R A 1928 Fields, currents and points *Phys. Rev.* **31** 901–9
- [8] Georghiou G E, Morrow R and Metaxas A C 1999 An improved finite element flux-corrected transport algorithm *J. Comput. Phys.* **149** 1–16
- [9] Grange F, Loiseau J F and Spyrou N 1995 Numerical and experimental determination of ionising front velocity in a DC point-to-plane corona discharge *J. Phys. D: Appl. Phys.* **113** 1619–29
- [10] Kim C Y and Goring D A 1971 Corona induced bonding of synthetic polymers to wood *J. Appl. Polymer Sci.* **15** 1357–64
- [11] Kulikovski A A 1997 Positive streamer between parallel plate electrodes in atmospheric pressure air *J. Phys. D: Appl. Phys.* **30** 441–50
- [12] Lama W L and Gallo C F 1974 Study of current pulses *J. Appl. Phys.* **45** 103–13
- [13] Lohner R, Morgan K, Peraire J and Vahdati M 1987 Finite element flux-corrected transport (FEM-FCT) for the Euler and Navier–Stokes equation *Int. J. Numerical Methods Fluids* **7** 1093–109
- [14] Meek J M and Craggs J D 1978 *Electrical Breakdown of Gases* (New York: Wiley)
- [15] Morrow R 1985 Theory of stepped pulses in negative corona discharges *Phys. Rev. A* **32** 3821–4
- [16] Morrow R 1987 Numerical modelling of time-dependent electrical breakdown in non-uniform electric fields *Proc. XVIII Int. Conf. Phenomena in Ionised Gases (Swansea, Wales)* ed W T Williams (Bristol: Adam Hilger) p 268
- [17] Morrow R 1991 Theory of positive corona in SF₆ due to a voltage impulse *IEEE Trans. Plasma Sci.* **19** 86–94
- [18] Morrow R and Lowke J J 1997 Streamer propagation in air *J. Phys. D: Appl. Phys.* **30** 614–27
- [19] Odrobina I and Cernak M 1995 Numerical simulation of streamer-cathode interaction *J. Appl. Phys.* **78** 3635–42
- [20] Penney G W and Hummert G T 1970 Photoionisation measurements in air, oxygen and nitrogen *J. Appl. Phys.* **41** 572–7
- [21] Raether H 1964 *Electron Avalanches and Breakdown in Gases* (London: Butterworths)
- [22] Raizer Y P 1991 *Gas Discharge Physics* (Berlin: Springer)
- [23] Roache P J 1972 *Computational Fluid Dynamics* (Albuquerque, NM: Hermosa)
- [24] Sato N 1980 Discharge current induced by the motion of charged particles *J. Phys. D: Appl. Phys.* **13** L3–6
- [25] Silvester P P and Ferrari R L 1990 *Finite Elements for Electrical Engineers* (Cambridge: Cambridge University Press)
- [26] Steinle P, Morrow R and Roberts A J 1989 Use of implicit and explicit flux-corrected transport algorithms in gas discharge problems involving non-uniform velocity fields *J. Comput. Phys.* **85** 493–9
- [27] Vitello P A, Penetrante B M and Bardsley J N 1994 Simulation of negative streamer dynamics in nitrogen *Phys. Rev. E* **49** 5574–98
- [28] Vitello P A, Penetrante B M and Bardsley J N 1993 Multi dimensional modeling of the dynamic morphology of streamer coronas *Non-Thermal Techniques for Pollution Control* part A, ed B M Penetrante and S E Schultheis (Berlin: Springer) pp 249–72
- [29] Wang M C and Kunhardt E E 1990 Streamer dynamics *Phys. Rev. A* **42** 2366–73
- [30] Yousfi M, Poinsignon A and Hamani A 1994 Finite element method for conservation equations in electrical gas discharge areas *J. Comput. Phys.* **113** 268–78